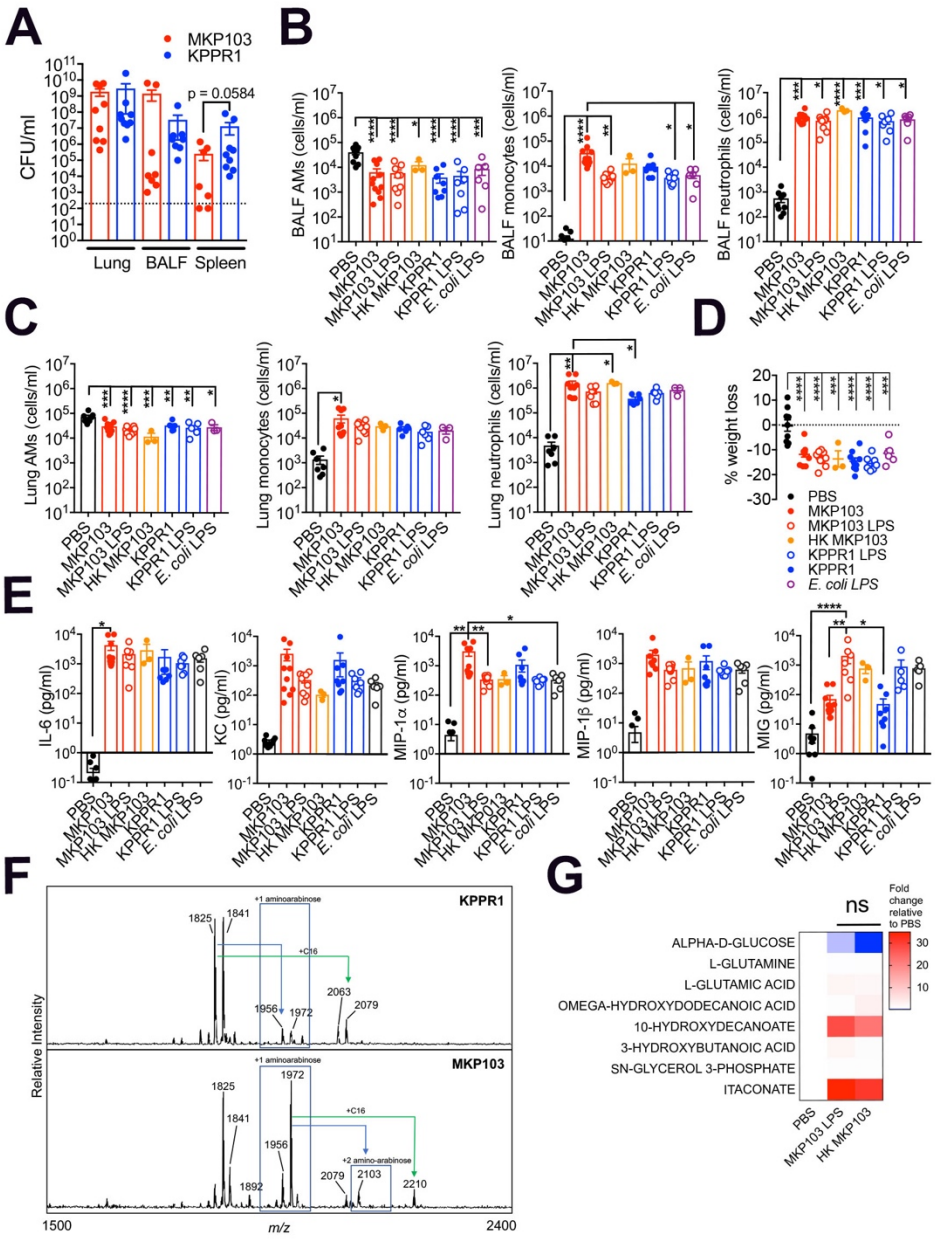

Figure S1. Metabolically active *K. pneumoniae* and PAMPs elicit similar airway immune responses, related to Figure 1 (B-C).

(A) Bacterial burden from the lung, BALF and spleen of WT BL/6 mice infected with MKP103 or KPPR1 48 h earlier, *n* = 9 mice per group respectively (3 independent experiments), statistical analysis by Mann Whitney U-test. The dotted line indicates the limit of detection.

(B-C) Innate immune cells (alveolar macrophages (AMs), monocytes and neutrophils) from the (B) BALF and (C) lungs of mice administered intranasally with PBS (*n* = 6 mice from 3 experiments), live (*n* = 9 mice from 3 experiments) or heat-killed (HK, *n* = 3 mice from 1 experiment) MKP103, live KPPR1 (*n* = 9 mice from 3 experiments) or purified LPS from MKP103, KPPR1 and *E. coli* (*n* = 7, 7 and 6 mice respectively from 3 experiments) 48 h earlier.

(D) Percentage of murine body weight loss 48 h post treatment.
(E) Cytokine measurements from the BALF of uninfected mice (*n* = 9 mice from 4 independent experiments) and mice treated with live (*n* = 11 mice from 4 independent experiments) or heat-killed MKP103 (*n* = 3 mice from 1 experiment), live KPPR1 (*n* = 8 mice from 3 independent experiments) or purified LPS from each Kp strain and *E. coli* (*n* = 9 mice stimulated with MKP103 LPS from 4 independent experiments, *n* = 7 mice stimulated with KPPR1 LPS from 3 independent experiments and *n* = 6 mice stimulated with *E. coli* LPS from 2 independent experiments).
(F) Negative ion mode matrix assisted laser desorption ionization-time of flight mass spectrometry (MALDI-TOF MS) lipid A spectra for KPPR1 and MKP103 (*n* = 1 biological sample per condition). The ions at *m/z* 1825 and 1841 correspond to lipid A with 2 and 3 hydroxyl groups respectively. Addition of 1 aminoarabinose group (Δ*m/z* 131) is observed in the hydroxylated lipid A of both KPPR1 and MKP103 (*m/z* 1956 and 1972). Addition of a second aminoarabinose group and a palmitate (C16, Δ*m/z* 238) to the triple hydroxylated lipid A of MKP103 is observed at *m/z* 2103 and 2210. KPPR1 has palmitate additions on both double and triple hydroxylated lipid A (*m/z* 2063 and 2079).
(G) Heatmap showing BALF metabolites from mice treated 48 h earlier with PBS (*n* = 3 mice from 1 experiment), MKP103 LPS (*n* = 2 mice from 1 experiment) or HK MKP103 (*n* = 3 mice from 1 experiment). The level of each metabolite in response to the different stimuli is compared by fold increase over the uninfected control (PBS); ns: not significant. Columns represent mean values ± SEM, statistical analysis for (B-E) was performed by one-way ANOVA; *P < 0.05, **P < 0.01, ***P < 0.001, ***P < 0.0001.

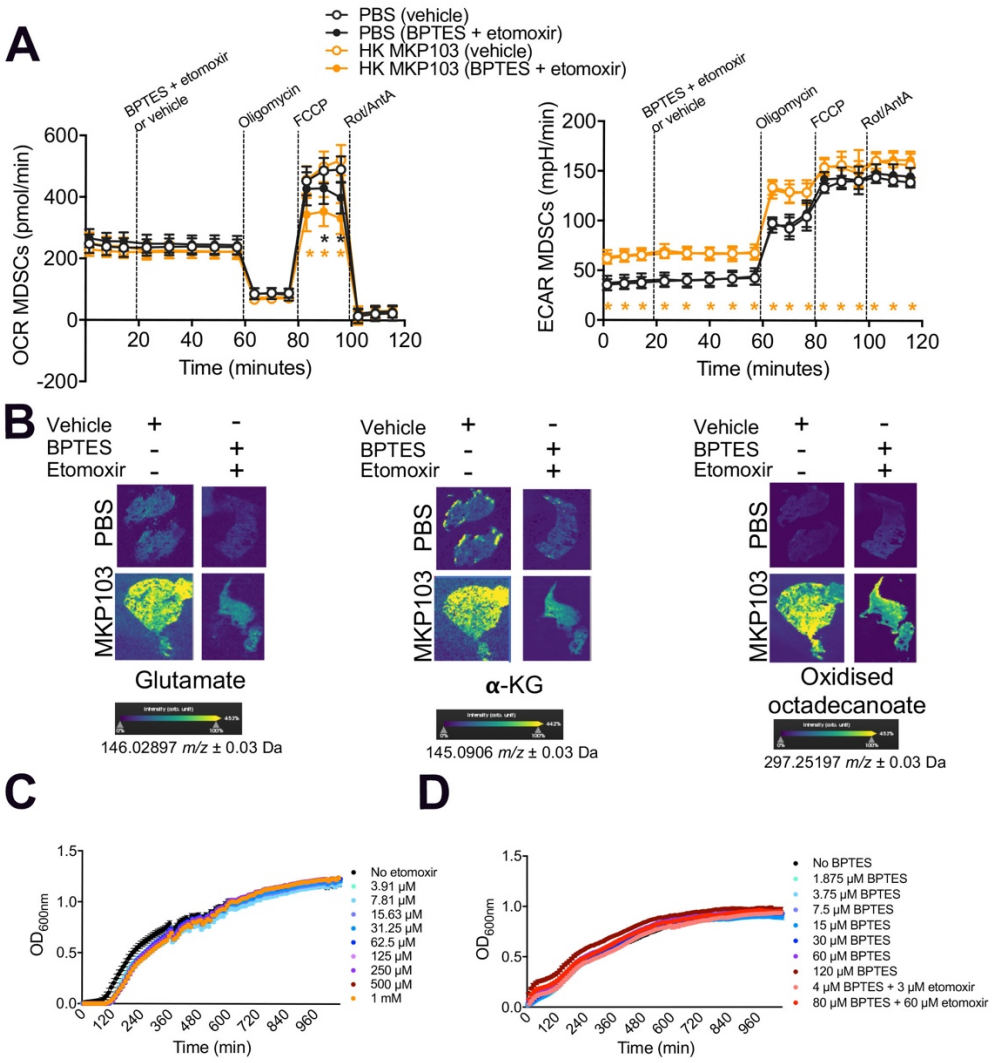

Figure S2. BPTES and etomoxir treatment inhibits host glutaminolysis and FAO-induced OXPHOS, related to Figure 2 (G-H).

(A) Oxidative phosphorylation (OXPHOS, left panel) and glycolysis (right panel) of murine bone marrow-derived MDSCs treated with PBS (control) or heat-killed (HK) MKP103, as measured by oxygen consumption rate (OCR) and extracellular acidification rate (ECAR) respectively, using the Seahorse extracellular flux analyzer. BPTES and etomoxir or the vehicle control, oligomycin, FCCP and rotenone/antimycin A were sequentially injected. Oligomycin inhibits ATP synthase, decreasing mitochondrial respiration (OCR). FCCP collapses the proton gradient, resulting in maximal OCR and the rotenone/antimycin A mixture shuts down mitochondrial respiration. The left panel shows that BPTES and etomoxir treatment inhibits maximal but not basal OCR in both uninfected and HK MKP103-treated cells without affecting glycolysis (right panel). Each data point is the mean ± SEM.; *n* = 2 biological samples (2 independent experiments), with 5 technical replicates per biological sample. The black asterisks denote statistical differences in uninfected MDSCs treated with BPTES and etomoxir versus the vehicle control; the orange asterisks denote differences in MDSCs stimulated with HK MKP103 and treated with BPTES and etomoxir versus the vehicle control; $P < 0.001$ by two-way ANOVA.

(B) DESI-MS spectral images of glutamate, α-KG and oxidized octadecenoate (FA derivative) in 10 μm lung sections from uninfected (PBS, *n* = 1 mouse) and MKP103-infected mice treated with the vehicle control (*n* = 1 mouse) or BPTES and etomoxir (*n* = 1 mouse).
(C-D) Growth of WT MKP103 in liquid LB culture with increasing concentration of (C) etomoxir and/or (D) BPTES, *n* = 2 biological samples (2 independent experiments), with 3 technical replicates per biological sample.

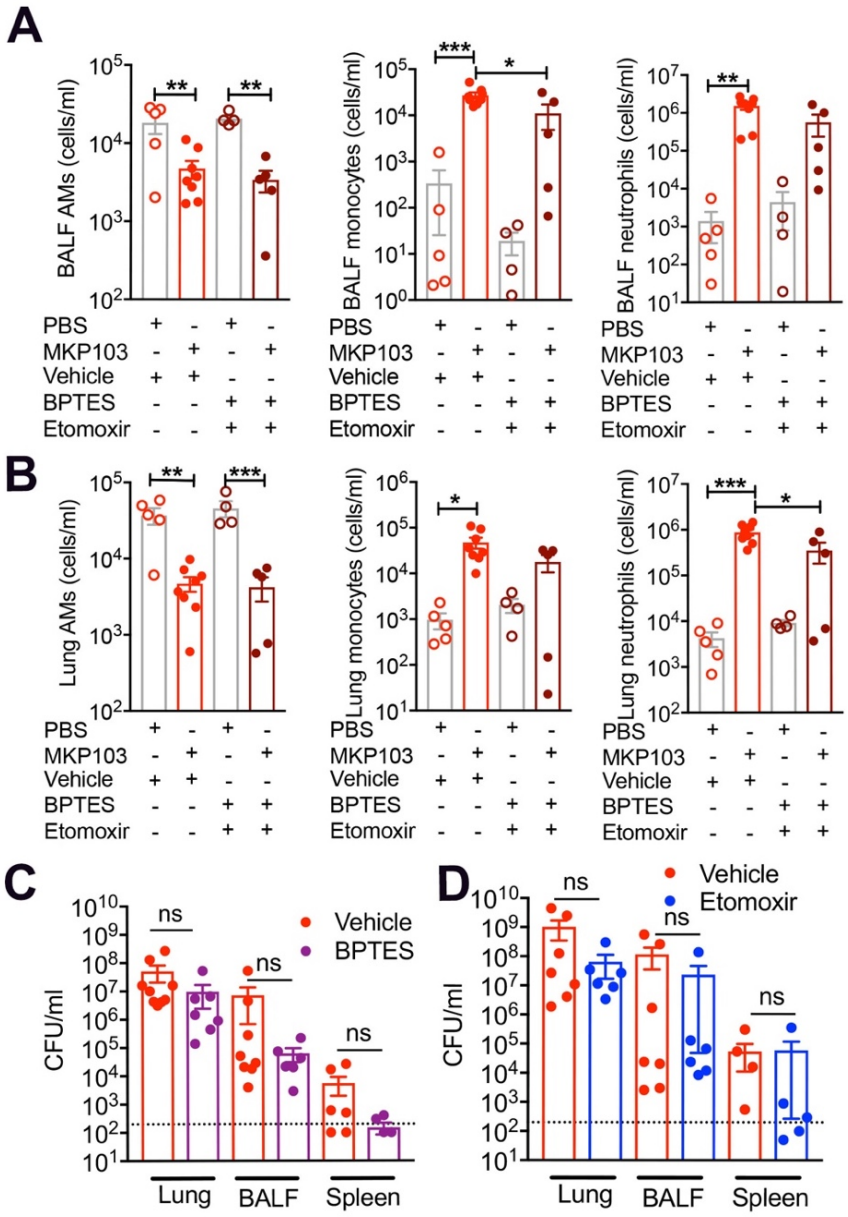

Figure S3. Inhibition of glutaminolysis and FAO has negligible effects on innate immune cell numbers in the airway, related to Figure 2 (G-H).

(A-B) Innate immune cells (alveolar macrophages (AMs), monocytes and neutrophils) from the (A) BALF and (B) lungs of uninfected (PBS) and MKP103-infected mice (48 h pi) treated with the vehicle control or the glutaminolysis and FAO inhibitors, BPTES and etomoxir, (n = 5, 8, 4 and 5 mice respectively from 2 experiments). Columns represent mean values ± SEM, statistical analysis for (A-B) was performed by one-way ANOVA; *P < 0.05, **P < 0.01, ***P < 0.001, ***P < 0.0001.

(C-D) MKP103 burden from the lung, BALF and spleen of MKP103-infected mice treated with the vehicle control versus (C) BPTES (n = 9 and 7 mice respectively from 2 experiments) or the vehicle control versus (D) etomoxir (n = 7 and 6 mice respectively from 2 experiments), statistical analysis by Mann Whitney U-test. The dotted line indicates the limit of detection.

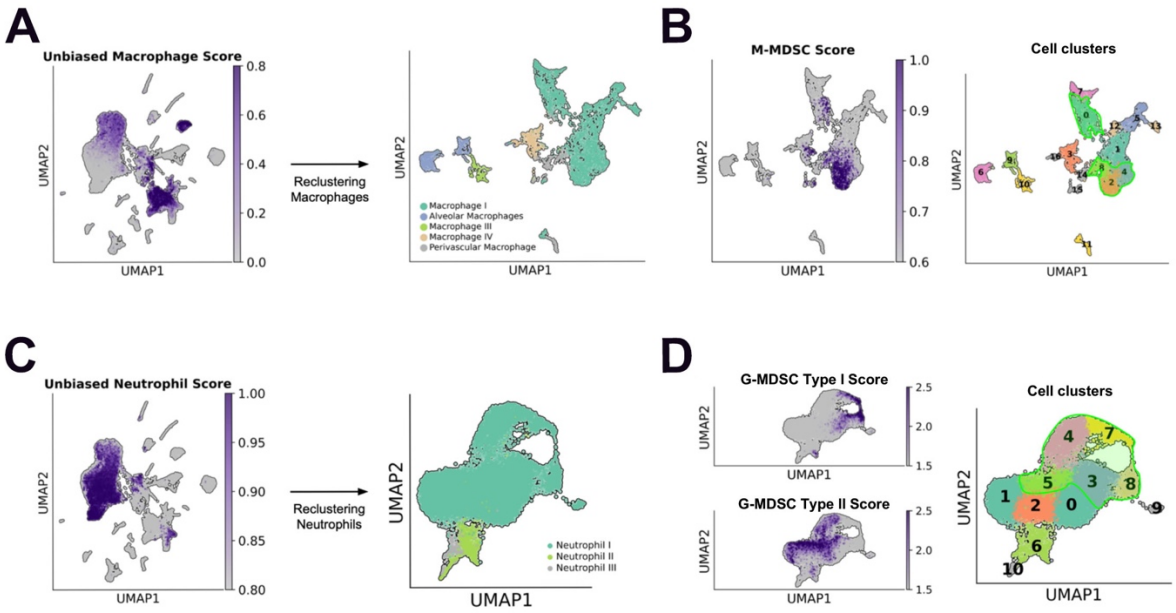

Figure S4. M and G-MDSC populations are interspersed with macrophage and neutrophil populations, related to Figure 3.

(A) Unbiased scoring of macrophage gene signatures (left), followed by subseting and reclustering of macrophage subpopulations (right).

(B) M-MDSC gene signature score (left, *IGTAM, LY6G, ARG1, NOS2, LY6C1*) for macrophage subpopulations and clusters selected for M-MDSC annotation and downstream analysis (right).

(C) Unbiased scoring of neutrophil gene signatures (left), followed by subseting and reclustering of neutrophil subpopulations (right).

(D) G-MDSC type I (*NGP, LTF, CD177, ANXA1, MMP8, S100A8, S100A9, CEBPE, LTB4R1, CYBB*) and type II (*CCL4, CCL3, CXCL2, CXCL3, SPP1, IL1B, NFKB1, SOCS3, MIF, KLF6, ATF3, PTGS2, XBP1*) gene signature scoring (left) for neutrophil clusters selected for G-MDSC annotation and downstream analysis (right).

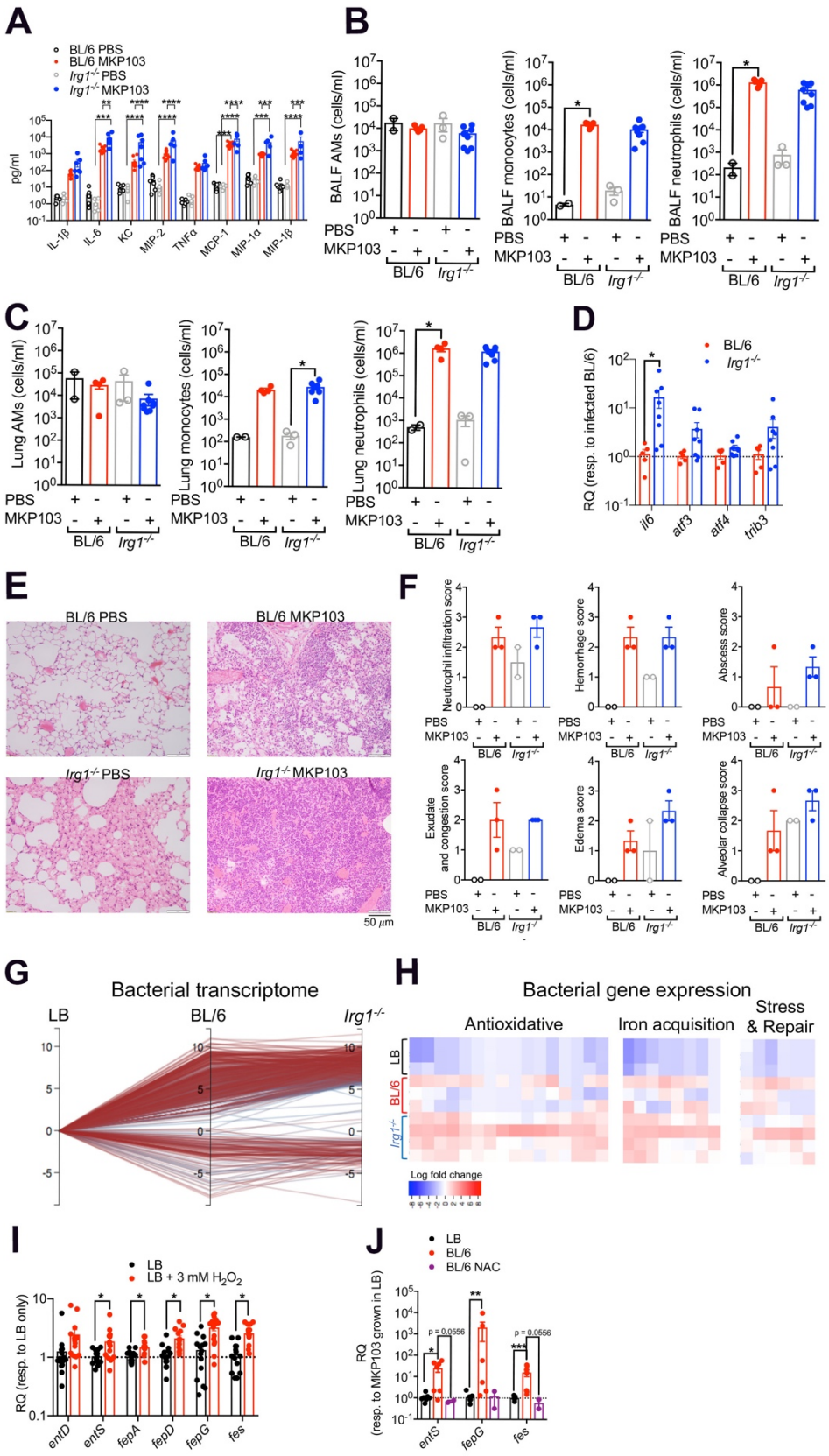
A
BL/6 PBS
BL/6 MKP103
Irg1-/- PBS
Irg1-/- MKP103
pg/ml
IL-1β
IL-6
KC
MIP-2
TNFα
MCP-1
MIP-1α
MIP-1β
B
BALF AMs (cells/ml)
BALF monocytes (cells/ml)
BALF neutrophils (cells/ml)
PBS
MKP103
BL/6
Irg1-/-
C
Lung AMs (cells/ml)
Lung monocytes (cells/ml)
Lung neutrophils (cells/ml)
D
RQ (resp. to infected BL/6)
il6
atf3
atf4
trib3
E
BL/6 PBS
BL/6 MKP103
Irg1-/- PBS
Irg1-/- MKP103
50 μm
F
Neutrophil infiltration score
Hemorrhage score
Abscess score
Exudate and congestion score
Edema score
Alveolar collapse score
G
Bacterial transcriptome
LB
BL/6
Irg1-/-
H
Bacterial gene expression
Antioxidative
Iron acquisition
Stress & Repair
Log fold change
I
LB
LB + 3 mM H2O2
RQ (resp. to LB only)
entD
entS
fepA
fepD
fepG
fes
J
LB
BL/6
BL/6 NAC
RQ (resp. to MKP103 grown in LB)
p = 0.0556
p = 0.0556

Figure S5. Itaconate influences both host and bacterial transcriptional responses, related to Figure 4.

(A) Cytokine measurements from the BALF of uninfected (PBS) and MKP103-infected WT or *Irg1*$^{-/-}$ mice (at 48 h pi), *n* = 7, 5, 10 and 7 mice respectively from 3 experiments.

(B-C) Innate immune cells (alveolar macrophages (AMs), monocytes and neutrophils) from the (B) BALF and (C) lungs of uninfected and infected WT BL/6 or *Irg1*$^{-/-}$ mice, *n* = 2, 5, 3 and 8 mice respectively from 3 experiments.

(D) Expression of murine *il6*, *atf3*, *atf4* and *trib3* from MKP103-infected WT BL/6 and *Irg1*$^{-/-}$ mice by qRT-PCR to validate the bulk-RNA seq results (Figure 3C), *n* = 5 and 8 mice respectively from 2 experiments, statistical analysis by Mann-Whitney U-test.

(E-F) Histopathology of MKP103 pneumonia demonstrating increased alveolar collapse and edema in H&E-stained lung sections from infected *Irg1*$^{-/-}$ (*n* = 3 mice from 2 experiments) versus WT BL/6 mice (*n* = 3 mice from 2 experiments) at 48 h pi. Lung sections from uninfected (PBS) WT BL/6 (*n* = 2 mice from 1 experiment) and *Irg1*$^{-/-}$ (*n* = 2 mice from 1 experiment) mice were included as controls. Scale bar (E): 50 μm.

(G) Parallel coordinates plot (using Degust) showing bacterial (MKP103) gene expression from *in vitro* LB liquid culture (*n* = 3 biological samples from 1 experiment) versus WT BL/6 (*n* = 3 biological samples from 1 experiment) and *Irg1*$^{-/-}$ (*n* = 4 biological samples from 1 experiment) mice, FDR cut-off of 0.05.

(H) Heatmap showing MKP103 expression of specific genes from (G) that are involved in counteracting oxidative stress or mediating iron acquisition or repair from stress.

(I-J) Expression of bacterial genes involved in iron acquisition from MKP103 grown in (I) LB with or without H_2O_2, *n* = 15 biological samples from 3 independent experiments or (J) harvested directly from the lungs of infected-WT BL/6 mice treated or untreated with NAC, *n* = 2 and 7 biological samples respectively from 2 experiments, by qRT-PCR. RQ, relative quantification to MKP103 grown in LB only.

Columns represent mean values ± SEM, statistical analysis for (A-C) was performed by one-way ANOVA; *P < 0.05, **P < 0.01, ***P < 0.001, ***P < 0.0001 and for (D), (I-J) was performed by Mann-Whitney U-test.